LiDR: Visible-Light-Communication-Assisted Dead Reckoning for Accurate Indoor Localization

Babar Hussain, *Member, IEEE*, Yiru Wang, *Graduate Student Member, IEEE*, Runzhou Chen, *Student Member, IEEE*, Hoi Chuen Cheng, and C. Patrick Yue, *Fellow, IEEE*

***Abstract*—Pedestrian dead reckoning (PDR) is an inertial navigation system that relies on smartphone sensors for estimating a pedestrian's step movements. However, such systems suffer from poor accuracy due to the drift and inherent noise in sensor readings. In addition, step size variation among pedestrians and device heterogeneity pose further challenges for building a scalable PDR system that can provide uniform performance across various devices and a diverse range of users. Visible light positioning (VLP), which uses LED lights with visible light communication (VLC) capability to provide high-accuracy localization, can achieve precision of a few cm. However, VLP systems suffer from practical limitations due to occasional line-of-sight (LOS) blockage and the sparse density of lighting in large-scale indoor venues. In this work, we propose a light-assisted dead reckoning (LiDR) system, which aims to address the problems of both VLP and PDR. It uses LED lighting as high-accuracy location landmarks to provide regular calibration for the PDR and estimates the individual pedestrians' step size for increased accuracy. In addition, a light-shape-based heading angle correction algorithm is proposed to reduce the heading angle error and further improve the accuracy. The system is implemented as an Android-based navigation application, with a digital map and cloud-based backend storage for location, device, and user-specific parameters. The real-time performance of the system is evaluated in a 450-m^2 lab and on a 150-m walking track. The experimental results demonstrate that with a maximum light spacing of 15 m, an overall average accuracy of < 0.7 m can be achieved for the whole system.**

***Index Terms*—Indoor positioning, optical camera communication (OCC), pedestrian dead reckoning (PDR), smartphones, visible light communication (VLC).**

Manuscript received 9 December 2021; revised 13 January 2022; accepted 6 February 2022. Date of publication 16 February 2022; date of current version 24 August 2022. This work was supported in part by the Foshan-HKUST Project through the Government of Foshan municipality under Grant FSUST20-SHCIRI05C; in part by the Project of Hetao Shenzhen-Hong Kong Science and Technology Innovation Cooperation Zone under Grant HZQB-KCZYB-2020083; in part by the Hong Kong Innovation and Technology Fund under Grant GHP/004/18SZ; and in part by the Hong Kong Research Grants Council under General Research Fund (GRF) under Project 16215620. *(Corresponding author: Babar Hussain.)*

Babar Hussain and C. Patrick Yue are with the HKUST Shenzhen-Hong Kong Collaborative Innovation Research Institute, Shenzhen 518000, China, and also with the Department of Electronic and Computer Engineering, The Hong Kong University of Science and Technology, Hong Kong (e-mail: bhussain@connect.ust.hk; eepatrick@ust.hk).

Yiru Wang and Runzhou Chen are with the Department of Electronic and Computer Engineering, The Hong Kong University of Science and Technology, Hong Kong (e-mail: ywangkf@connect.ust.hk; rchenas@connect.ust.hk).

Hoi Chuen Cheng is with LiPHY Communications Limited, Hong Kong (e-mail: johnny@liphy.io).

Digital Object Identifier 10.1109/JIOT.2022.3151664

I. Introduction

HIGH-ACCURACY indoor navigation is important for a wide range of futuristic Internet of Things (IoT) applications for consumers and industry [1]. For instance, indoor positioning systems (IPSs) are the principal component of intelligent location-based services (LBSs) in smart cities, for deployment in locations, such as airports, train stations, shopping malls, and hospitals, and with target applications that include navigation, asset tracking, workforce management, and location-based emergency response and automation. However, with the global positioning system (GPS) as the only useable outdoors, there is no single positioning technology that can work indoors with acceptable accuracy, pervasiveness, and affordable implementation cost.

Pedestrian dead reckoning (PDR), which relies on the built-in sensors of smartphones, is a key component of nearly every indoor positioning technology, as it does not require any infrastructure other than a smartphone [2], [3]. However, since PDR relies on estimating positions based on step count, its accuracy relies on the correct estimation of pedestrian step size and heading direction, which are both challenging to estimate correctly. Step size estimation suffers due to variation in pedestrians' step sizes and walking patterns. Meanwhile, the heading direction is usually estimated via the built-in smartphone compass that relies on a magnetometer and accelerometer and suffers from errors due to its sensitivity to buildings' metallic structure and nearby metallic objects and electrical appliances. Therefore, PDR positioning accumulates error with every step and must be calibrated using other IPS technologies, such as WiFi [4]–[7], Bluetooth [8], [9], geomagnetics [10], [11], acoustics [12], or sensor-based landmark detection [13].

The problem is that these other IPS technologies and landmarks themselves lack accuracy and precision. For instance, RF-based solutions suffer from multipath effects and shadowing in indoor environments, which lead to poor accuracy and stability [14], [15]. In addition, these systems are not suitable for deployment in sensitive environments due to severe electromagnetic interference and health concerns [16]. Meanwhile, WiFi-, geomagnetic-, and landmark-based solutions are sensitive to the changing indoor environment and hence require regular site surveying for fingerprint and landmark updating in order to maintain acceptable accuracy. Hence, when PDR is combined with these IPSs, the position can only be corrected up to the baseline accuracy of the employed IPS, while key issues related to step length, heading angle, and pedestrian and

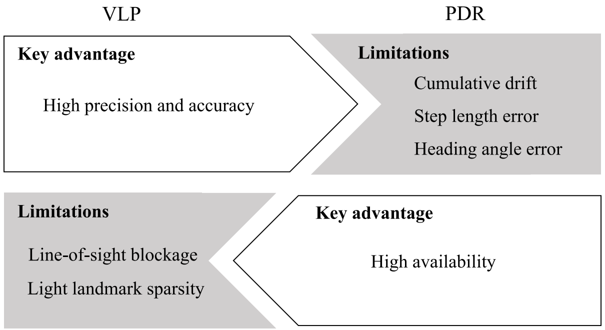

Fig. 1. Complementary advantages and limitations of VLP and PDR.

device heterogeneity are either left unresolved or are solved using other computationally complex methods [13], [17]–[19]. Therefore, in order to realize cm-level accuracy for pervasive indoor applications, a cm-level baseline IPS technology must be employed.

Visible light communication (VLC), which uses ordinary LED lighting to broadcast information is a promising technology for providing data communication and indoor positioning for IoT applications [20], [21]. Thanks to their low-cost, energy efficiency, and reliability, LEDs continue to be widely used in applications including lighting, display, and signage [22], creating opportunities for VLC deployment in a wide range of IoT applications [23]–[25]. Furthermore, thanks to the rolling shutter effect of CMOS image sensors, VLC can be made ubiquitously available in consumer smartphones using optical camera communication (OCC) [26], [27]. The accuracy of OCC-based visible light positioning (VLP) systems can be as high as a few cm [28]–[31].

However, VLP systems have an inherent drawback due to the line-of-sight (LOS) property of VLC. They require that the light must be received by the smartphone camera at all times, but this is not possible in practical scenarios for several reasons. First, the lighting density is determined based on the illumination requirements in the area and follow a standard, for instance, EN 12464 [32]. Therefore, it is not practical to install more LEDs in an area than required. To achieve optimum lux levels indoors, the spacing required between adjacent lights is usually larger than the smartphone camera's Field of View (FoV), leading to occasional blind spots in the camera view during walking. In addition, areas, such as hallways and corridors, have much lower illumination requirements, leaving a distance of several footsteps between adjacent lighting fixtures. Second, in large-scale public venues, it may not be feasible to enable VLC in all lighting fixtures due to cost and logistics requirements, leaving fewer lights for VLP. Therefore, it is imperative that VLP be combined with PDR for uninterrupted coverage. At the same time, high-accuracy VLP is ideal for resolving the above-discussed challenges associated with PDR. This complementary nature of the advantages and limitations of PDR and VLP is illustrated in Fig. 1.

A few prior works have proposed to combine VLP with PDR to extend the coverage of IPSs [21], [33]–[35]. However, these works merely employ VLP as landmark to correct the accumulated position error of PDR, without addressing the key challenges of PDR, which include step length estimation, heading error correction, user diversity, and device heterogeneity. In this work, we propose to use high-accuracy VLP to not only correct the PDR accumulated error but also to calibrate the step size and heading direction of pedestrians while addressing the sensor inaccuracy, user diversity, and device dependency issues, without using any map constraints or sensor-based landmarks as proposed in previous works. We implement our algorithm as a complete indoor navigation application with a digital map to measure the real-time performance of our proposed solution.

Our contributions are summarized as follows.

1) We design light-assisted dead reckoning (LiDR), a PDR-based IPS that uses VLP for pedestrian step length estimation and heading angle calibration while addressing the device heterogeneity and user diversity challenges of PDR.
2) We propose a method that uses the high-accuracy VLP positioning signal from a single LED source to instantaneously estimate pedestrian step length while passing under the light.
3) We propose an algorithm to correct the heading angle error of PDR by utilizing the geometrical features of the LED lighting shape.
4) We describe the system architecture for implementing our proposed system on an Android-based indoor navigation application with a digital map-based frontend and cloud-based backend server containing user-, device-, and light-specific parameters. We demonstrate the real-time performance of our application in a 15×30 m^2 experimental lab, achieving < 0.7-m precision.

The remainder of this article is organized as follows. Section II presents the relevant literature review. The design methodology and implementation details are discussed in Section III, and experimental results and discussions are presented in Section IV. Finally, a conclusion is drawn in Section V.

II. Related Work

In this section, related works on PDR step length estimation and heading angle calibration are presented first, followed by a review of works on the use of VLP with PDR. A summary of these works along with their limitations is presented in Table I.

A. Step Length Estimation

Step length can be estimated either using direct acceleration integration or through indirect methods such as biomechanical models or statistical methods [17]. Direct methods require double integration of acceleration to find displacement, which results in sensor error being integrated and causing large deviation in measurements [17], [36].

Biomechanical methods rely on modeling the direct relationship between acceleration and step length. For instance, [37] proposed to use the mean of the acceleration in each step to calculate step length. Similarly, [38] determined the step length based on the cyclic nature of walking by measuring the arms' swing. Weinberg's model [39] is popular for

TABLE I
PDR CHALLENGES, RELATED WORKS, AND THEIR LIMITATIONS

PDR challenges	Technology or methods used	Limitations
(1) Position calibration	WiFi [4–7]	Requires fingerprinting and performance varies across devices
	Bluetooth [8], [9]	Requires additional hardware installation and performance varies across devices
	Geomagnetics [10], [11]	Requires fingerprinting and susceptible to environment changes
	Acoustics [12]	Susceptible to reflection and background noise
	Landmark graph [13]	Requires empirical modeling to build a landmark graph
	Map constraints [49]	Requires extensive computation on map to determine walkable area and fencing
	Crowd sourcing [51]	Works with at least one of the above, privacy concerns due to location sharing
(2) Step length estimation	Double integration [17], [36]	Large errors due to integration of sensor noise
	Biomechanical methods [37], [38], [39]	Poor accuracy due to diversity in pedestrians' step size
	Context-based methods [40], [41]	Wrong estimation of context leads to large positioning errors
	Walking mode [42]	Walking patterns and behaviors vary from person to person
	Neural network-based methods [43–45]	Computationally inefficient to implement on a smartphone
	Optical flow method [18]	Complex image processing and dependency on environment
(3) Heading angle correction	Sensor fusion [2], [19], [46–48]	Computationally complex with limited accuracy
	Map aided heading correction [49]	Only applicable in certain locations, e.g., straight corridors
	RSSI-based using linear regression [50]	Only works when walking in a straight line

hand-held smartphones, estimating step length based on the maximum and minimum peaks of vertical acceleration, and it has been shown to perform well in smartphone-based PDR [2].

Context-based methods [40], [41] and regression-based methods [42] rely on probabilistic estimation of walking patterns and smartphone carrying state, based on feature extraction from sensor data. However, a wrong estimation of context or carrying state could lead to large errors in step length estimation, as it is not possible to accurately model the diversity of walking patterns and smartphone carrying states of pedestrians.

The use of neural network-based methods for step length estimation has also been proposed in [43] and [44]. However, these methods are expensive in both implementation complexity and hardware requirements.

The use of optical flow for estimating the step length of pedestrians using the backside camera of a smartphone was proposed in [18]. However, this method involves complex image processing and is not suitable for VLP systems that utilize the frontside camera and ceiling-mounted lights.

The aforementioned methods focus only on solving a generic model to be applied to pedestrians, without taking into consideration the device heterogeneity or the diversity in human walking patterns. Recently, a neural network-based personalized step length estimation method [45] that addresses the heterogeneity of pedestrian step length via online learning was proposed. However, this method requires magnetic fingerprint-based map matching, which makes the computation heavy on the edge device. In addition, neural network-based online methods require additional computation power on the cloud side, making the whole system very complex and costly to implement. In contrast, our proposed system can instantaneously estimate the step length of a pedestrian walking under VLC-modulated lights without relying on any computationally complex trajectory mapping or neural networks.

B. Heading Angle Estimation

In addition to the wrong step size, the other major source of error in PDR navigation systems is the heading angle, which is primarily due to the sensitivity of the smartphone compass to magnetic distortions caused by building structures and nearby metallic objects in indoor environments. The proposed solutions in the literature generally aim at solving this problem by either using only the smartphone's built-in sensors to mitigate the effects of magnetic distortions or using map- and trajectory-based heading correction methods.

Several methods rely only on using sensor data to find the heading direction. For instance, [2] proposed to alternatively use a magnetometer or gyroscope to avoid magnetic disturbances at the corners while turning 90°. WalkCompass [19] combines data from the smartphone's inertial sensors to minimize the magnetic interference and corrects the heading direction error by up to 8° of accuracy. In [46], an experimental heuristic approach for determining the heading of the user without using magnetometers was proposed. It uses an experimentally determined threshold for each user. Similarly, [47] used a normalized gravity vector from a smartphone rotation vector sensor within one step to obtain the heading direction during various smartphone carrying modes. Wang *et al.* [48] proposed to use multihead convolutional

TABLE II
COMPARISON OF RELATED WORKS ON USING VLP WITH PDR

Ref	VLP Algorithm	Platform	Implementation	Utilizes VLP for			Considered	
				PDR Calibration	Step Length Estimation	Heading Angle Correction	Device Heterogeneity	User Diversity
[21]	RSS	Simulation	NA	✓	×	×	×	×
[33]	RSS	MCU & Foot-mounted Device	Offline	✓	×	×	×	×
[34]	Image sensor-based 3D position	Smartphone	Offline	✓	×	×	×	×
[35]	ID-detection only	Smartphone	Not mentioned	✓	×	×	×	×
Our Work	**Image sensor-based 3D position**	**Smartphone**	**Real-time**	✓	✓	✓	✓	✓

neural networks (CNNs) to identify the walking pattern of pedestrians and used the principal component analysis (PCA) approach with a gyroscope-based relative heading.

Map-aided heading correction relies on identifying paths on corridors, matching pedestrian trajectories with navigation paths and avoiding wall crossovers [13], [49]. Gu *et al.* [13] proposed to correct the heading by constraining the user's location between two landmarks in a straight corridor for calibration, followed by gyroscope-only heading estimation. Similarly, [50] proposed to correct the heading error in PDR using a position estimate acquired through WiFi RSSI using linear regression while the user is walking in a straight line. In [51], an indoor–outdoor positioning system using crowd-sensing data was proposed, where the heading error is corrected by matching the PDR traces during the indoor–outdoor transition based on detecting landmarks at the gate.

The limitation of all of the above methods is that they rely either on using sensor fusion to identify the heading direction or pedestrian trajectory matching on a map, which makes the methods computationally complex and only applicable in certain locations. On the other hand, our proposed method uses light geometry to instantaneously calibrate the heading while the pedestrian is walking under VLC-modulated lights, at a comparatively lower computational cost.

C. VLP With PDR

The proposed use of PDR with VLP in the literature has been primarily aimed at eliminating the LOS blockage and extending the coverage. In [33], an RSS-based VLP system was fused with a foot-mounted PDR device. However, the system was tested in an impractically small area of less than 3 m $\times$ 3 m with a high density of seven VLC lights. A smartphone-based high-accuracy VLP system with PDR was proposed in [34]. However, the scope of the experiment was limited to a straight corridor with large heading errors in PDR on the return path. In [35], OCC-based light ID detection was used to correct PDR error within a predefined radius of the LED coverage area without realizing high-precision VLP. Similarly, [21] proposed a simulation model for VLC RSSI-based positioning combined with PDR for locating photodiode (PD)-based receiving devices. Although their simulation results claimed a high accuracy of 4.3 cm, the lack of experimental verification and requirement of a PD-based receiver makes it unsuitable for practical consumer smartphone-based IPS deployment.

In addition to the lack of practical deployment considerations and limited experimental verification, the aforementioned works use VLP as a PDR calibration tool without addressing the practical limitations of PDR. On the other hand, our focus is on using VLP to resolve limitations, including step length differences, heading angle error, device heterogeneity, and user diversity. The contribution of our work in comparison to the aforementioned literature is illustrated in Table II.

According to the above summary of related works, the essential advantages of LiDR lie in its scalable approach in comparison to existing methods, making it ready for practical deployment. The three key comparative advantages are the following. First, the step size estimation can be enabled for any number of heterogeneous users and smartphones without any pretraining or postdeployment maintenance. Second, the heading angle can be corrected, without any map constraints or sensor fusion, at a very low additional computation cost. Finally, LiDR can be implemented as an indoor navigation application with real-time performance on ordinary smartphones.

III. METHODOLOGY

In this section, we first present the overview of the whole system by briefly introducing all the key components, followed by detailed description of each algorithm, including, VLP, dead reckoning, step length estimation, and heading angle correction. Finally, we present the software application architecture to describe integration of all components.

A. System Overview

The system architecture of LiDR is shown in Fig. 2, where a person is shown walking with a smartphone under

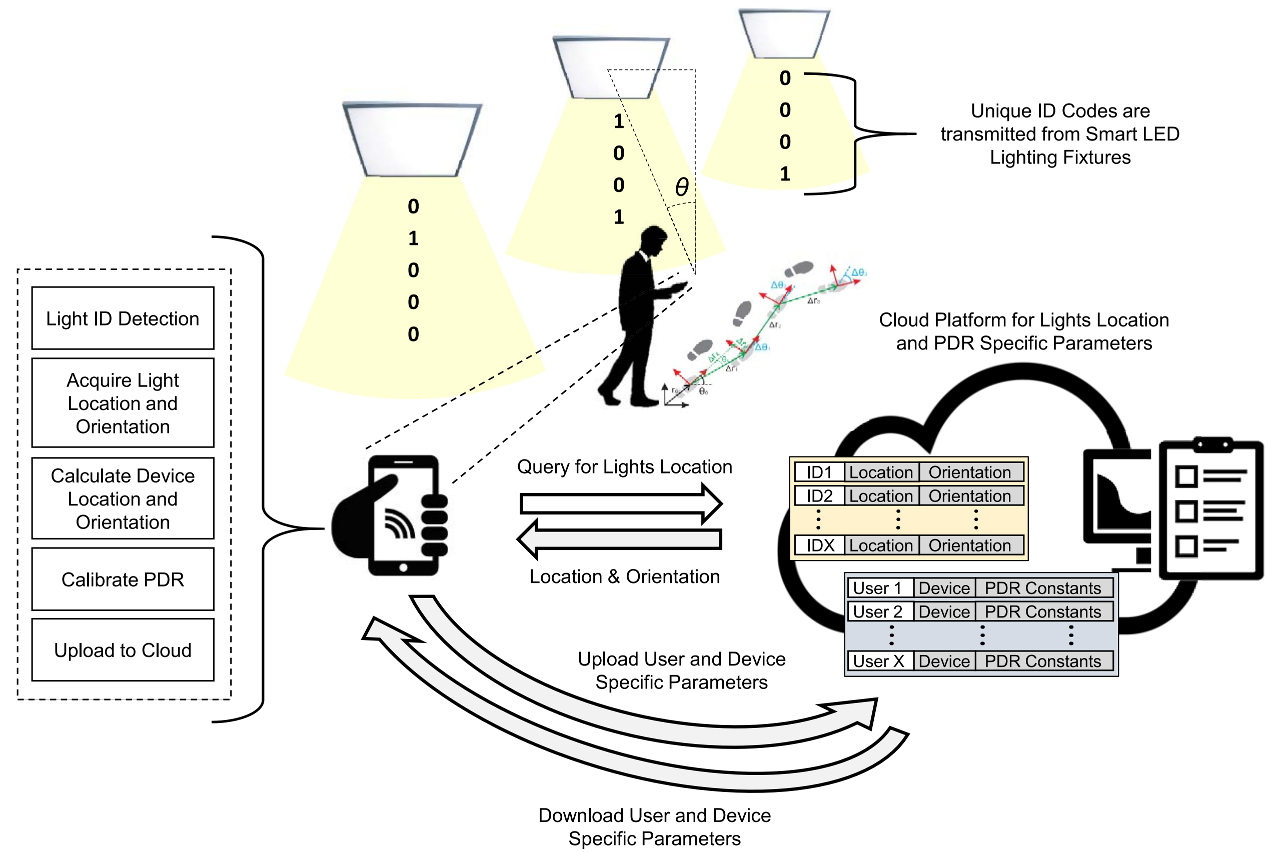

Fig. 2. System overview. Combined usage of image sensor-based VLP and PDR with cloud-controlled backend database to provide high-accuracy indoor localization.

VLC-modulated smart LED lights transmitting unique identifiers (IDs). As the person passes under an LED light, his position, orientation, and walking step length are calibrated via high-accuracy image sensor-based VLP, but when the person is walking in between the lights, such that there is no light seen by the smartphone camera, PDR is used to estimate his location. The light configuration information including, light ID, location in the building, and orientation, is stored in the cloud along with the building's digital map database. The PDR- and VLP-related device-specific parameters are also stored and continuously updated in the cloud for later access and sharing among users and devices.

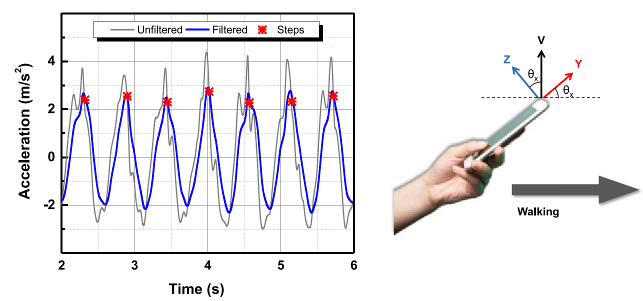

Fig. 3. Vertical acceleration waveform and smartphone holding state while walking.

B. Dead Reckoning

There are several ways of tracking smartphone acceleration to detect pedestrian steps, which involve detecting the smartphone holding state and pedestrians' walking mode [52]. In this work, we will primarily focus on the case where the user is actively navigating while holding the phone in hand, and looking at the screen. Therefore, we choose to use the vertical acceleration for step detection [2]. Since the smartphone is likely to be held at a slightly tilted angle in this case, as illustrated in Fig. 3, the smartphone's pitch angle needs to be considered to effectively extract the vertical acceleration component from the y- and z-axis of acceleration. The smartphone's 3-D acceleration w.r.t the world frame acc_w is given as

$$\text{acc}_W = R_{x,y,z} \ * \ \text{acc}_{x,y,z} \tag{1}$$

where $R_{x,y,z}$ is the 3-D rotation matrix of the smartphone w.r.t to the world reference frame and $\text{acc}_{x,y,z}$ is the 3-D acceleration w.r.t the smartphone's reference frame. The vertical acceleration component acc_v can be extracted as

$$\begin{bmatrix} \text{acc}_x \\ \text{acc}_y \\ \text{acc}_v \end{bmatrix} = R_z R_y R_x \ * \begin{bmatrix} \text{acc}_x \\ \text{acc}_y \\ \text{acc}_z \end{bmatrix}. \tag{2}$$

However, if we only consider the smartphone's tilt angle around the x-axis, i.e., pitch angle, we can simplify it as follows:

$$\begin{bmatrix} \mathrm{acc}_x \\ \mathrm{acc}_y \\ \mathrm{acc}_v \end{bmatrix} = R_x * \begin{bmatrix} \mathrm{acc}_x \\ \mathrm{acc}_y \\ \mathrm{acc}_z \end{bmatrix} \tag{3}$$

$$\begin{bmatrix} \mathrm{acc}_x \\ \mathrm{acc}_y \\ \mathrm{acc}_v \end{bmatrix} = \begin{bmatrix} 1 & 0 & 0 \\ 0 & -\cos\theta_x & \sin\theta_x \\ 0 & \sin\theta_x & \cos\theta_x \end{bmatrix} * \begin{bmatrix} \mathrm{acc}_x \\ \mathrm{acc}_y \\ \mathrm{acc}_z \end{bmatrix} \tag{4}$$

which leads to the following expression:

$$\mathrm{acc}_v = \mathrm{acc}_y \sin\theta_x + \mathrm{acc}_z \cos\theta_x. \tag{5}$$

However, the accelerometer data can have both noise and multiple spikes due to differences in the walking patterns of the pedestrians. Therefore, in order to suppress the spikes, we must apply a low pass filter on the accelerometer data with a cut off frequency of 2.5 Hz, which is assumed to be the maximum walking step rate of a pedestrian in normal circumstances. The employed filter is a moving average-based attenuator with the output expression given as follows:

$$y_t = \begin{cases} x_t, & t = 1 \\ x_t\alpha_t + (\alpha_t - 1)y_{t-1}, & t > 1 \end{cases} \tag{6}$$

The attenuation factor α is calculated as follows:

$$\alpha_t = (\tau_t - \tau_{t-1})/\left[T + (\tau_t - \tau_{t-1})\right] \tag{7}$$

where τ_t and τ_{t-1} represent the system clock at instance t and $t-1$, respectively, and T is the time constant of the filter. The filtered vertical acceleration waveform is shown in Fig. 3.

The step detection is performed by tracking the positive and negative peaks of vertically filtered accelerations, hereafter, referred to as peaks and valleys. In order to ensure the peaks and valleys belong to a valid step, we ensure that the difference between the peak and valley is greater than a threshold and the time difference between the last and current step is no more than the period of the maximum walking step frequency ($\mathrm{WF}_{\max}$). The step condition is shown in the following equation:

$$t_k^{\mathrm{step}} = \left\{ t \;\middle|\; \begin{matrix} \left(a_{t=t^{\mathrm{peak}}} - a_{t=t^{\mathrm{valley}}}\right) > \epsilon_{\mathrm{step}} \\ \left(t - t_{k-1}^{\mathrm{step}}\right) > 1/WF_{\max} \end{matrix} \right\} \tag{8}$$

where t_k^{step} is the time of the kth step, ϵ_{step} is the peak to valley threshold, $a_{t=t^{\mathrm{peak}}}$ and $a_{t=t^{\mathrm{valley}}}$ represent the peak and valley accelerations, respectively, and are defined in the following equations:

$$t^{\mathrm{peak}} = \left\{t \;\middle|\; a_t > a_{t+1},\ a_t > a_{t-i},\ 1 \le i \le n_p \right\} \tag{9}$$

$$t^{\mathrm{valley}} = \{t \mid a_t < a_{t+1},\ a_t < a_{t-i},\ 1 \le i \le n_v \}. \tag{10}$$

We set $n_p = 2$ and $n_v = 1$, respectively. The walking frequency WF is calculated as follows:

$$WF = N/\sum_{k=2}^{N}\left(t_k^{\mathrm{step}} - t_{k-1}^{\mathrm{step}}\right) \tag{11}$$

where $N = 5$ to consider only the five most recent steps to continuously adapt to the changing walking speed of the pedestrian.

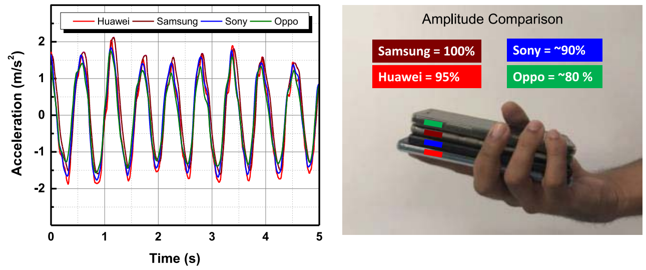

Fig. 4. Comparison of accelerometer waveform recorded from various Android devices.

In order to consider the impact of device diversity on step detection, we conducted an experiment to compare accelerometer waveforms on four different models and brands of smartphones. The data were collected while simultaneously holding all the smartphones in the hand to ensure every device would experience the same acceleration, as shown in Fig. 4. The comparison shows that the waveforms of all the devices are nearly identical, except minor differences in amplitude, with the Samsung smartphone recording the largest amplitude while the Oppo device had the smallest amplitude among the four devices. These results indicate that the PDR detection algorithm can perform identically on these smartphones if the step detection thresholds are tuned according to the relative acceleration amplitude of each device. Therefore, in order to address these variations, we use a variable step detection threshold ϵ_{step} defined as follows:

$$\epsilon_{\mathrm{step}} = \frac{\sum_k^{k-N}\left(a_{t=t_k^{\mathrm{peak}}} - a_{t=t_k^{\mathrm{valley}}}\right)}{2N}. \tag{12}$$

Here, $N = 5$ is kept the same as in (11).

C. Visible Light Positioning

Very high-accuracy VLP can be realized using OCC. With the light ID being detected via OCC, the relative position between the smartphone and the LED light can be calculated via the angle of arrival based on the camera's projective geometry. Fig. 5 shows the basic principle for VLP via the camera's projection, which is given as

$$p_c = C[R|T]\,P_w \tag{13}$$

where p_c is a point's coordinates on an image, with its real-world coordinates being P_w, C is the camera intrinsic matrix and is found through camera calibration, and R and T are the rotation and translation matrices of the smartphone, respectively. R is calculated by the smartphone gyroscope and is available through the Android sensor API. T determines the real-world location of the smartphone w.r.t to the point P_w. The equation can be rewritten as

$$s\begin{bmatrix} u \\ v \\ 1 \end{bmatrix} = \begin{bmatrix} fx & 0 & c_x \\ 0 & fy & c_y \\ 0 & 0 & 1 \end{bmatrix}[R|T]\begin{bmatrix} X \\ Y \\ Z \\ 1 \end{bmatrix}. \tag{14}$$

Here, s is the scaling factor of image point's homogenous coordinates. For VLP, the real-world position of the center of the LED is known. Therefore, if we know the

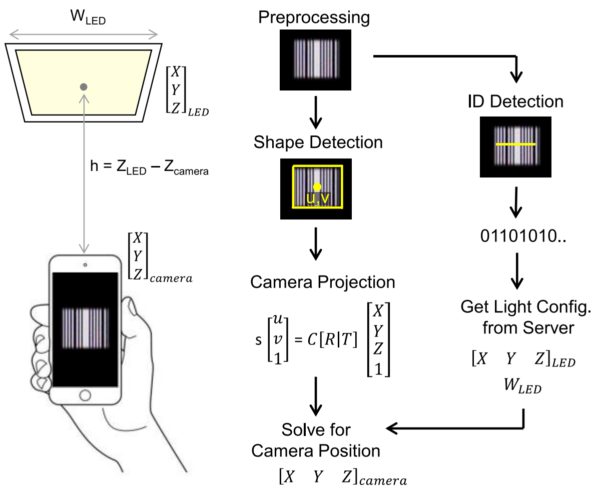

Fig. 5. Visible light positioning using optical camera communication: (a) image capture, (b) processing steps.

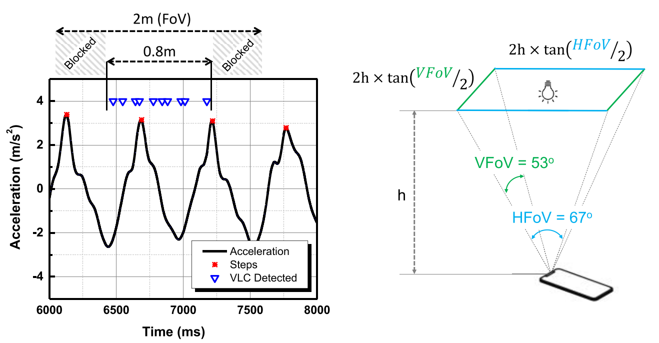

Fig. 6. Step size estimation via partially blocked FoV during pedestrian walking. (a) Position tracking during effective FoV. (b) FoV and height of ceiling.

center coordinates of the LED's projection on the image (u, v), we can solve (14) for T to find the relative position of the smartphone w.r.t the LED's center.

D. Step-Length Estimation

Step-length estimation via VLP requires the smartphone camera to see the LED light continuously for a period of at least twice the step rate, such that the position at the start and end of the step can be detected to measure the step length accurately. Therefore, the wider the FoV of the smartphone camera, the more reliable the step length estimate will be. The available FoV of the camera is dependent on the height of the ceiling, which is fixed for a particular indoor venue. For instance, in a venue with a ceiling height of 2.7 m, an average-height pedestrian holds the smartphone at about 1.5 m from the ceiling, which will give a coverage range of 2 m for a typical front camera FoV of 67°, as shown in Fig. 6(b). However, as shown in Fig. 7, while the person is holding the phone in front of his body, half of the FoV is blocked by the person's own head, which can reduce the effective FoV. In addition, the natural holding position of the smartphone is slightly tilted to allow

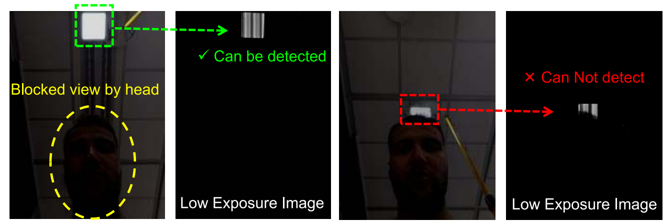

Fig. 7. Front camera view with its corresponding low-exposure image captured while the pedestrian is walking under the light and holding the phone in front, at two instances. (a) Time = t. (b) Time = t + 300 ms.

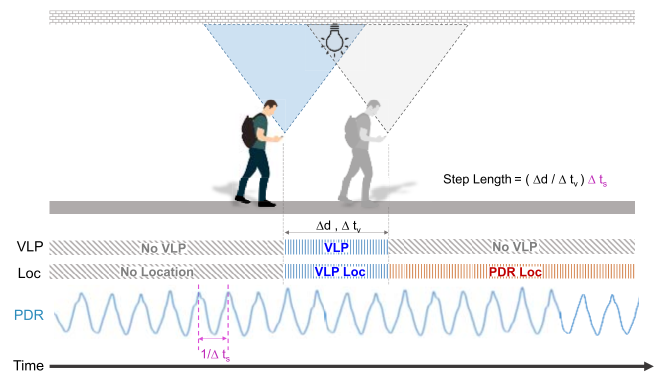

Fig. 8. Using VLP for measuring step size of a pedestrian.

the person to see the full face of the screen while walking, which results in a pitch angle, it can be up to 30° or higher. This leads to an even smaller FoV and thus, can reduce the range over which the step length can be estimated.

We conducted an experiment by having a pedestrian carry an Android smartphone (Huawei P30 pro) with a FoV of 67° and walk under a 2.7-m high ceiling light, and recorded the results, as shown in Fig. 6(a). The measurements show that the effective area of 2 m FoV is reduced to 0.8 m with only 1 step recorded during that interval. This leads to an important conclusion that it is not feasible to directly estimate the step size by measuring the VLP distance traveled during the two consecutive step detection peaks. Instead, a more reliable approach is to measure the walking speed of the person and use the step rate to determine the step length.

The concept of using VLP to measure the step length of the pedestrian is presented in Fig. 8. When a pedestrian passes under the light while holding the smartphone, his position can be tracked using VLP with high accuracy (∼10 cm) and a fast update rate of up to 30 frames/s for a period of time t_v, while the smartphone camera can see the light. The distance traveled during this period (d_v) can then be used to calculate the walking speed of the pedestrian. With the information of the step interval available, the step length of the pedestrian can be estimated by the product of the walking speed and step interval. The location tracked by the VLP at time t is given as

$$\text{Loc}_t^{\text{VLC}} = (x_t, y_t). \tag{15}$$

The walking speed WS_t of the pedestrian can be measured using the first and last VLP location of the recent consecutive VLP location outputs, which is given as

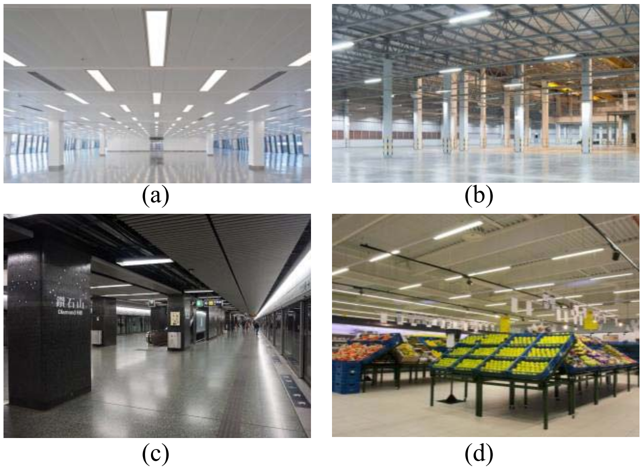

Fig. 9. Rectangular lighting at commercial and industrial venues. (a) Office. (b) Warehouse. (c) Metrostation. (d) Supermarket.

$$WS_t = \frac{d\left(\text{Loc}_1^{\text{VLC}}, \text{Loc}_N^{\text{VLC}}\right)}{t_{k=N} - t_{k=1}}\Bigg|\, t > (t_{k=N} \; + 2\Delta t_{\text{VLC}}) \tag{16}$$

where Δt_{VLC} is the VLP location output rate and $\text{Loc}_N^{\text{VLC}}$ is the last VLP location captured by the smartphone camera. The step length can then be found as

$$\text{Step Size} = \frac{WS_t}{WF_t}. \tag{17}$$

The walking speed and step size of a pedestrian can vary as they walk out of the VLP coverage area and before they arrive under the next light for recalibration. Therefore, we can employ Weingberg's [39] acceleration amplitude-based step size estimation equation to extract the subject-dependent constant from the measured step size in (17). Weingberg's step size estimation equation is given as

$$\text{Step Size} = k\sqrt[4]{\left(a_{t=t^{\text{peak}}} - a_{t=t^{\text{valley}}}\right)}. \tag{18}$$

With our predetermined step size, we can find k as follows:

$$k = \frac{\frac{\sqrt{(x_N - x_1)^2 + (y_N - y_1)^2}}{t_{k=N} - t_{k=1}}}{\sqrt[4]{\left(a_{t=t^{\text{peak}}} - a_{t=t^{\text{valley}}}\right)}}. \tag{19}$$

According to the experimentation performed in [53], the distance measurement accuracy of Weinberg's model is less than 1 m for a distance of up to 10 m. Therefore, if a VLC light is available every 10 m, the target accuracy of < 1 m can be achieved.

E. Heading Angle Correction

Heading angle correction is a very challenging problem to solve for accurate PDR as the smartphone's compass can be easily influenced by the building's structure and nearby metal. However, with image sensor-based VLP being used for accurate positioning, the heading angle calibration can also be performed simultaneously using the geometry of the LED light.

Since the majority of the lighting used at commercial and industrial venues are in a rectangular shape, as shown in Fig. 9, it makes intuitive sense that light shape can be utilized for precise estimation of the heading of pedestrians while they are passing under the light. In addition, since the image processing and signal decoding is already being performed for the location estimate of the pedestrian, the heading angle correction can be incorporated into the algorithm at a relatively low additional computational cost.

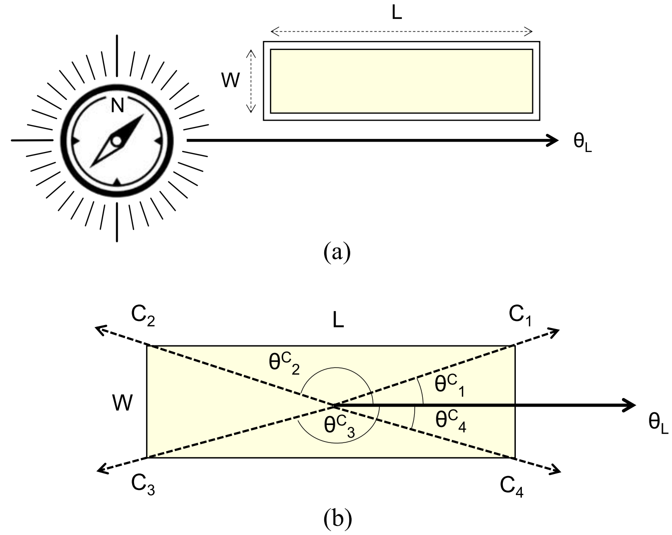

Fig. 10. Heading angle estimation from rectangular light shape. (a) Measuring the real-world orientation and size of light. (b) Calculating the corner angles of light.

The algorithm relies on the lights' geometry and installation orientation information, which can be stored in the building's map database and can be made available through the cloud. The width (W) and length (L) determine the shape of the rectangle, whereas the angle θ_L specifies the compass orientation along the longer dimension of the rectangle. It is important to note that both square-shaped light panels and tube lights are a special case of a rectangular shape, with $W = L$ and $W << L$, respectively. Since the order of the corners from the detected image cannot be determined absolutely, the algorithm is only used to correct the heading angle to the true orientation of the nearest corner, as explained below. The steps involved in angle correction are described as follows.

1) Setting up Light Configuration Database: Geometry-based angle correction requires the light's shape and orientation information to be preloaded in the database. As in Fig. 10 (a), for each light, the database must hold its light ID, width (W), length (L), and installation orientation (θ_L) along the longer dimension, i.e., L given in degrees from the north.

2) Orientation of Corners: Based on a light's orientation θ_L, we can find the orientation of each corner from the center, as shown in Fig. 10 (b). If the orientation angle for the light's ith corner is denoted as θ_i^C, then the four corner angles of a rectangular light can be calculated as

$$\theta_i^C = \begin{cases} \theta_L + \arctan\frac{W}{L}, & i = 1 \\ \theta_L + \arctan\frac{W}{L} + 2\arctan\frac{L}{W}, & i = 2 \\ \theta_L - \arctan\frac{W}{L} - 2\arctan\frac{L}{W}, & i = 3 \\ \theta_L - \arctan\frac{W}{L}, & i = 4. \end{cases} \tag{20}$$

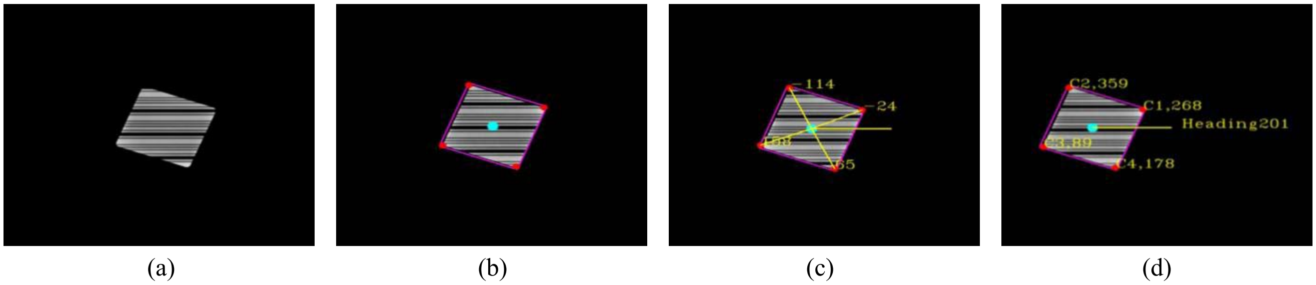

Fig. 11. Image processing steps for heading angle correction. (a) Grayscale converted image of a square downlight LED panel. (b) Corner and median detection. (c) Corner angles w.r.t to smartphone axis. (d) Estimated world orientation of corners and smartphone heading.

These corner angles' expressions can be simplified for a square light, where $W = L$, as

$$\theta_i^C = \begin{cases} \theta_L + \pi/4, & i = 1 \\ \theta_L + 3\pi/4, & i = 2 \\ \theta_L - \pi/4, & i = 3 \\ \theta_L - 3\pi/4, & i = 4. \end{cases} \tag{21}$$

For a tube-light, where $W << L$, we can further simplify the expression to approximate the rectangular shape as a line with two corners, as

$$\theta_i^C = \begin{cases} \theta_L, & i = 1 \\ \theta_L + \pi, & i = 2. \end{cases} \tag{22}$$

3) Angle Correction: During the image processing for VLP, the light shape and corner information is already available, as shown in Fig. 11(b). The angle correction can be applied by finding the estimated orientation of each corner based on the smartphone's compass and minimizing the difference between the estimated orientation and the real-world orientation calculated in the previous step. We find the angle between the positive y-axis of the smartphone and each corner, denoted as C_i, add it to the smartphone compass reading, and find the estimated orientation of each corner φ_i^C , as follows:

$$\varphi_i^C = \theta_{\text{compass}} + \angle C_i, \ i = a, b, c, d. \tag{23}$$

Here, a, b, c, and d denote the subscripts for the corners of the light's projection in an image, as opposed to 1, 2, 3, and 4, which denote the corners in the real world. However, the order of correspondence between the image corners and real-world corners is not known, but can be found by minimizing the difference, shown as

$$i = k \Big| \min\Big(\theta_k^C - \varphi_i^C\Big) i = a, b, c, d, 1 \leq k \leq 4. \tag{24}$$

Hence, we can find the correction offset to add to the smartphone compass to correct the heading error as

$$\theta_{\text{offset}} = \min\Big(\theta_k^C - \varphi_i^C\Big). \tag{25}$$

The maximum tolerable compass error that can be corrected by the proposed method depends on the number of possible orientations of the smartphone that could lead to identical images of the light. For instance, a square-shaped light could have an identical projection when viewed from four different orientation angles of the smartphone with a difference of 90°. Hence, the maximum tolerable compass error for a square light is 45°. Similarly, for a rectangular-shaped light, with $L > W$, there are only two possible orientations of the smartphone, with a difference of 180°, and hence, the maximum tolerable compass error is 90°. This correction capability is in good agreement with the measured data of various smartphones in [54], which reported an 80% compass error of $< 45°$.

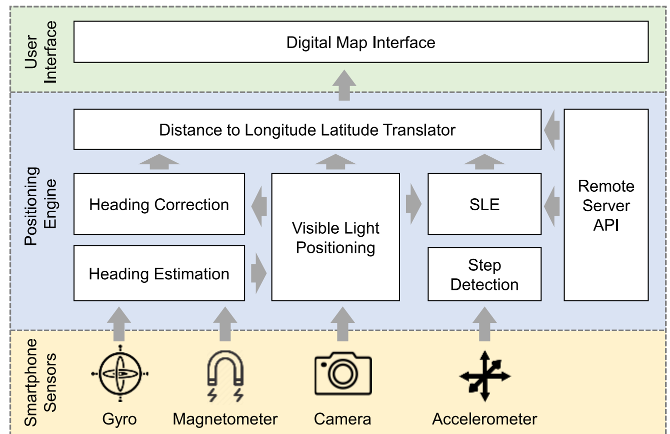

Fig. 12. Indoor navigation application architecture.

F. Software Integration

The complete indoor positioning function is realized in an Android-based indoor navigation application, which shows the real-time location of the user on a digital map. The application architecture is shown in Fig. 12, which highlights the software integration of various sensors, positioning engine, and application front-end user interface. The data from the sensors are collected through their respective APIs and used by the positioning engine for absolute position and orientation calculation. Meanwhile, the remote server API provides lighting configuration information to the positioning engine, which includes lights' GPS coordinates, dimensions, and installation orientation. This configuration information is used for heading estimation and relative position calculation by the distance to longitude and latitude translation block, which provides the location coordinates for the digital map to update the user's location cursor.

IV. Experiment and Evaluation

In this section, we first evaluate the performance of each algorithm individually, starting with VLP, then combining VLP and dead reckoning for step-length estimation, and followed

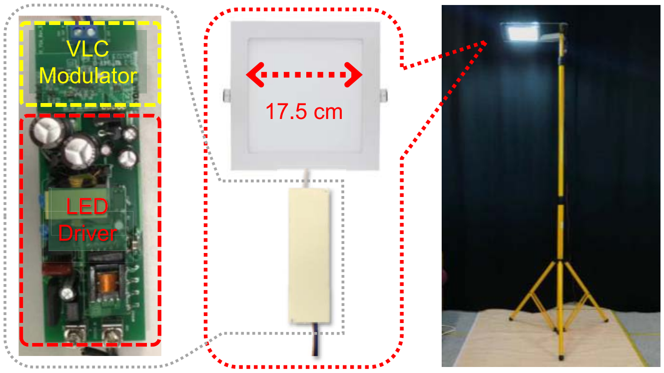

Fig. 13. Square-shaped smart LED light mounted on an adjustable light pole.

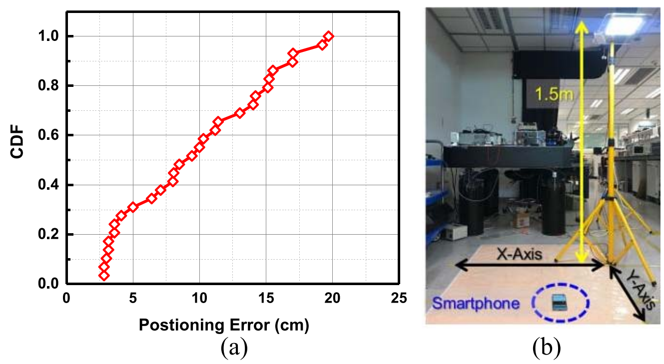

Fig. 14. VLP accuracy measurement. (a) Measurement setup. (b) CDF of positioning error.

by the heading angle correction algorithm. Finally, we evaluate the LiDR indoor navigation application to characterize the positioning accuracy performance of the whole system.

The experiments were carried out in our laboratory with an area of $\sim$ 450 m^2. For testing and evaluation, we ran our LiDR indoor navigation application on an Android smartphone (Huawei P30 Pro). For lighting hardware, LED light panels mounted on a pole with adjustable height and embedded with a VLC modulator were used as smart LED lights. The smart LEDs consist of a power supply unit and a down-light square panel with an area of 17.5 cm $\times$ 17.5 cm, as shown in Fig. 13. The LED power supply comprises a standard 18-W constant-current LED driver with an MCU-based VLC modulator module integrated on a single PCB. The VLC modulator for each LED is programmed to a unique ID to identify its installation location with building and floor information, its orientation, and its size in the cloud database.

A. Visible Light Positioning

The accuracy of VLP directly impacts the accuracy of the PDR step size estimation and calibration. Therefore, it is the most critical factor in determining the overall performance and reliability of our proposed LiDR system. Fig. 14(b) shows the measurement setup, consisting of a 1.5-m tall light pole with a square LED light panel mounted at the top and a Cartesian coordinates chart pasted on the floor with the LED's center positioned at the origin. For an average ceiling height of 2.7 m, an average-height pedestrian usually holds the smartphone at about 1.5-m distance from the ceiling. Therefore, the height of the LED is set to be 1.5 m in the experiment. During the recording of positioning data, the smartphone is placed at points on the grids each 20 cm apart while tilting the phone at various random tilt angles. The pitch and roll angles are varied up to 30° and 20°, respectively, which cover the natural smartphone holding state of pedestrians while walking during navigation. The magnitude of the positioning error at each point is calculated by measuring the difference between the ground truth and the measured position. The cumulative density function (CDF) of the positioning error, shown in Fig. 14(a), indicates that the mean positioning error is about 8 cm with maximum-recorded error of less than 20 cm.

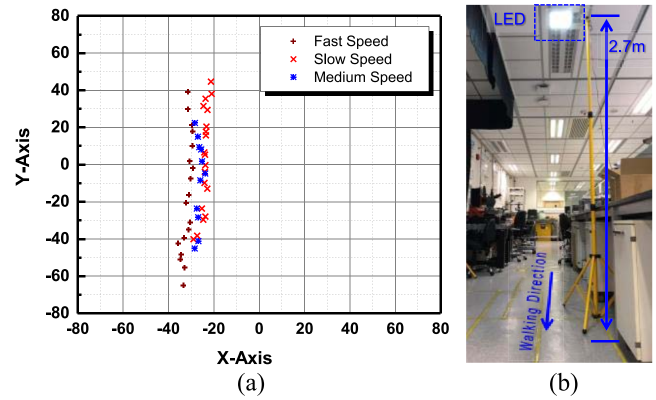

Fig. 15. Step length estimation experiment. (a) VLP tracking results at three different walking speeds. (b) Setup.

B. Step-Length Estimation

To verify the accuracy of the step length estimation, we conducted an experiment by placing the LED in a corridor of about 9-m length at a height of 2.7 m from the floor, as shown in Fig. 15(b). The pedestrian held the smartphone in hand and walked under the light at three different speeds 50 times to have his step length measured by the Android application running the proposed algorithm. To provide a reference for actual step size during the walk, we calculated the average step length of the person based on the number of steps taken during the 9-m distance. Fig. 15(a) shows the $x - y$ Cartesian graph of the measured positions of the pedestrian at three different walking speeds in an area of 1.6 m $\times$ 1.6 m with the LED at the origin. The graph shows that on average, an area of 80 cm is covered by the high accuracy VLP estimate and can cover less than two steps of the pedestrian during the walk.

The CDF of the step length estimation error for the aforementioned experiment is shown in Fig. 16. The mean step length error is 3.8 cm with a maximum-recorded error of less than 9 cm. This leads to an inference that in order to keep the average positioning error < 1 m, a VLC light must be deployed every 26 steps, which leads to an average 15-m walking distance between each light, assuming an average pedestrian step length of 60 cm.

C. Heading Angle Correction

The effect of tilt on the average estimated heading error is shown in Fig. 17. When the smartphone is tilted, the square shape of the light gets distorted and results in error in the heading angle estimation. In the experiment, we measured

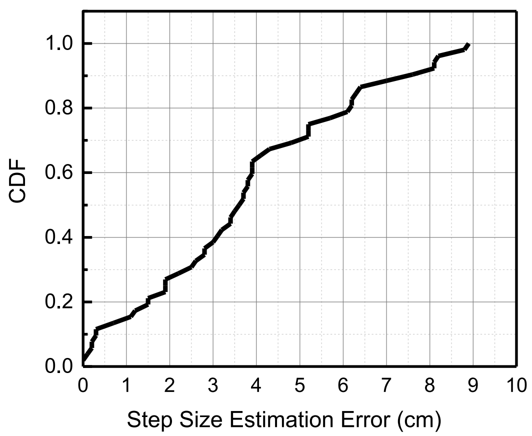

Fig. 16. CDF of step size measurement error.

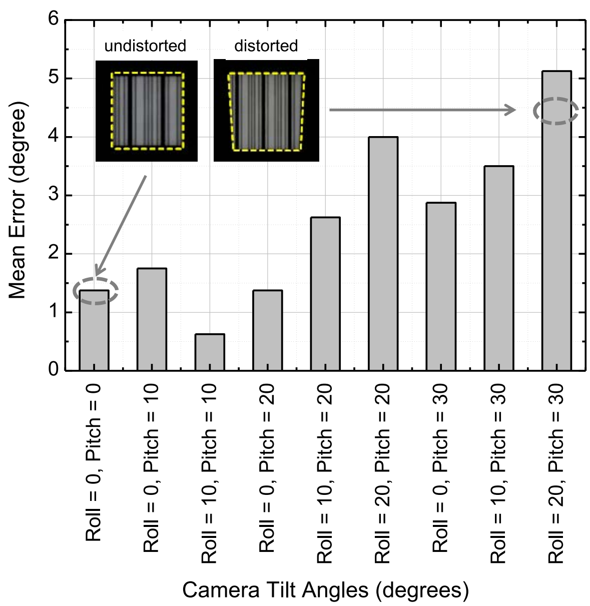

Fig. 17. Heading angle estimation error due to camera tilt.

the heading angle estimation error for various smartphone tilt angles by varying the roll and pitch angles from 0° to 30° and 20°, respectively. The average heading angle estimation error is directly proportional to the amount of tilt, with maximum recorded error being 5° for the maximum tilt.

Fig. 18 shows the heading angle estimation measurement setup and the CDF plot of heading angle estimation error for various degrees of tilt, with maximum roll and pitch being 20° and 30°, respectively. The graph shows that the mean heading angle estimation error is 2.5°, with the 90th percentile error being less than 5°.

D. Computation Timing

While the output timing of the VLP algorithm is highly critical to the correct step length estimation, it is computationally the most complex part of the algorithm as it involves image processing and VLC ID decoding, which takes a relatively larger number of computations to complete. Therefore, it is imperative that the positioning result of the VLP algorithm

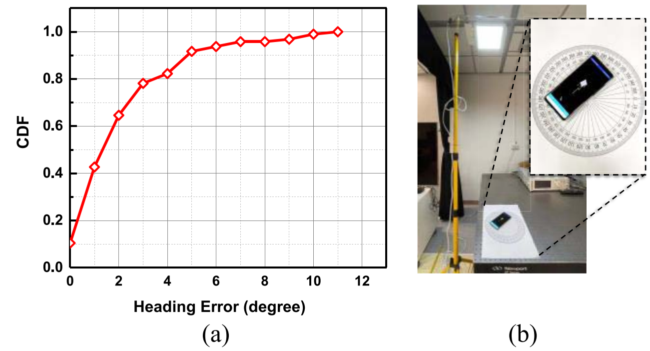

Fig. 18. VLC heading angle estimation. (a) CDF of heading estimation error. (b) Measurement setup.

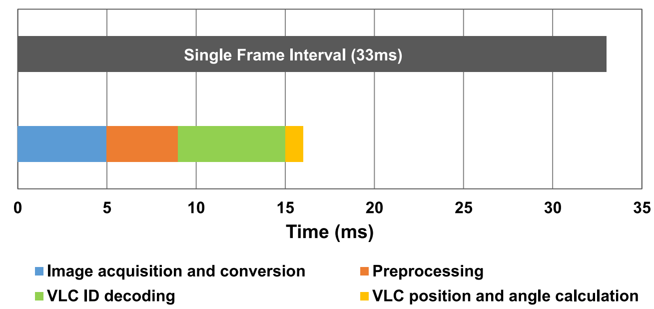

Fig. 19. VLP algorithm computation time.

from one captured camera frame is available before the camera captures the next frame. The frame capture rate of the smartphone camera is 30 frames/s, which leads to an available interval of 33 ms for the image conversion, preprocessing, VLC ID decoding, and position and angle calculation. In order to verify the timing performance of the algorithm, we ran the VLP computation algorithm for several instances while the person holding the smartphone was standing under the light and the positioning result was being consecutively output. We then recorded the average frame processing time with a moving average window of about 200 frames. The results are shown in Fig. 19, indicating that the average frame processing time is about 16 ms, which is about 50% of the available time and hence, can safely meet the timing requirements for the position output rate.

E. Indoor Navigation Performance

The overall performance of the LiDR indoor navigation system is evaluated in our testing lab with a testing area of 15 m × 30 m. We choose three tracks with varying lengths and light spacing to see the impact of light density on the overall accuracy of the system. Fig. 20 shows the measurement results of the three tracks with a total track length of 40, 120, and 150 m, with average light spacing of 5, 10, and 15 m, respectively. The results show that the shortest track, shown in Fig. 20(a), can achieve a very high accuracy due to the frequent calibration of the position, step size, and heading angle using VLP landmarks and keep a mean position error of less than 0.3 m. As the light spacing increases, the position error also increases, with the 10-m light spacing in the track of

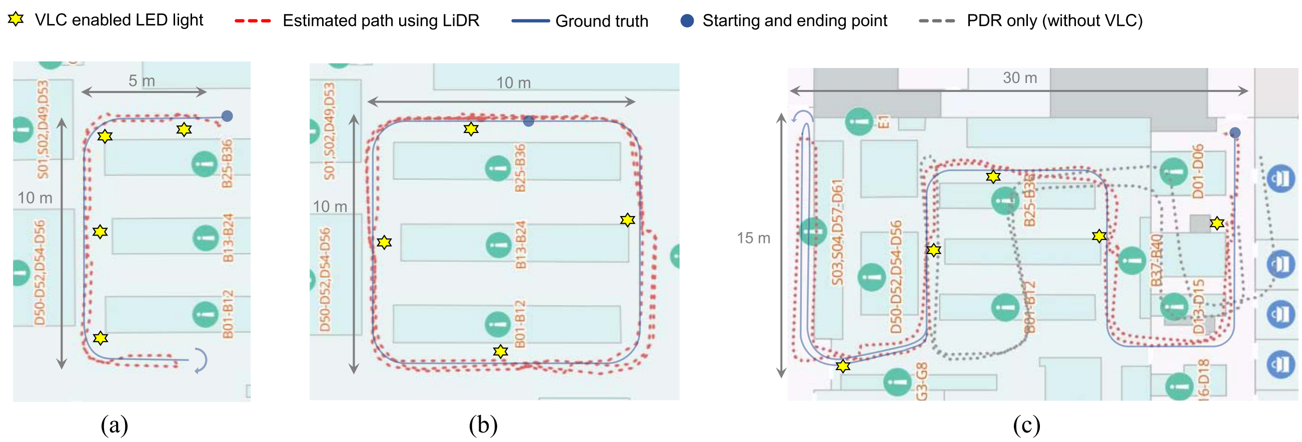

Fig. 20. Measurement results of the proposed LiDR-based indoor navigation application. (a) Track length = 40 m (two loops), Avg. light spacing = 5 m, and mean position error < 0.3 m. (b) Track length = 120 m (three loops), Avg. light spacing = 10 m, and mean position error < 0.5 m. (c) Track length = 150 m (two loops), Avg. light spacing = 15 m, and mean position error < 0.7 m.

TABLE III
PERFORMANCE COMPARISON OF VLP-BASED PDR METHODS

Ref	VLP Algorithm	Implementation	Testing Area	Light Spacing	Walking Track		Position Error
					Total Length	No. of Turns	
[34]	Image sensor-based 3D position	Smartphone (offline)	0.3×12 m^2	12 m	24 m	1	< 1 m*
[35]	ID-detection only	Smartphone	34×60 m^2	8 m	94 m	1	< 1 m
Our Work	**Image sensor-based 3D position**	**Smartphone (real-time)**	**30×15 m^2**	**~ 15 m**	**150 m**	**13**	**< 0.7 m**

* Estimated from the measurement data provided in the reference.

Fig. 20(b) achieving a 0.5-m accuracy and the 15-m light spacing in the track of Fig. 20(c) achieving an accuracy of < 0.7 m. This indicates that in order to deploy a VLP and PDR-based indoor navigation system, the quantity of VLP landmarks can be determined based on the required positioning accuracy in the target area. For comparison, a measurement is conducted with PDR only using a fixed step size and starting point and without VLC-based step length or heading correction along the track, as shown in Fig. 20(c). It can be observed that due to the erroneous heading and step size, the measurement drifts quite far from the true path, validating the necessity of VLP.

The results are further compared with related works on VLP-based PDR methods in Table III. For comparison, we only choose works on smartphone-based implementations and exclude [21] and [33] for being simulation-based and foot-mounted sensor-based, respectively. The comparison reveals that the proposed algorithm for using VLP to simultaneously calibrate position, step size, and heading angle can significantly improve the accuracy while needing fewer VLP landmarks, thereby reducing the requirement of VLP landmark density and providing more immunity to LOS blockage. In addition, high accuracy on a relatively longer walking track with a large number of turns further demonstrate the robustness of the algorithm.

V. CONCLUSION

In this work, a VLC-assisted PDR-based indoor navigation system is presented. Our proposed system, LiDR, uses a high-accuracy VLP location estimate to instantaneously calibrate PDR position and pedestrian step length as a user passes under a VLC-embedded LED light. To further improve the accuracy, we propose a method to use light shape and geometry features for heading angle calibration at a relatively low computational cost as compared to other sensor fusion-based methods proposed in the literature. In addition, we reveal a system architecture for implementing LiDR on a smartphone application with a digital map-based frontend and a cloud-based backend for the user and device parameter storage to support a diverse range of devices and users. We evaluated the real-time performance of the smartphone application in our lab, and demonstrated that the proposed system can achieve a precision of < 0.7 m with a light density of as low as one light every 15 m.

Although the proposed method has demonstrated a very high positioning accuracy, a few limitations could be addressed to improve the robustness. First, the heading angle correction algorithm does not work on circular lights as there are no geometrical features to help with the orientation. To overcome this limitation, the trajectory between two consecutive circular lights could be exploited to correct the heading. Second, the proposed method does not consider the scenario that the phone is inside a pocket. In such cases, even though high-accuracy positioning may not be necessary since the user is not actively looking at the phone, an auxiliary positioning technology, such as Bluetooth or WiFi, could be used to estimate the location with moderate accuracy. Therefore, in our future work, we plan to integrate Bluetooth beacon-based location tracking for such scenarios where VLC is not available for prolonged periods of time.

References

[1] F. Zafari, I. Papapanagiotou, and K. Christidis, "Microlocation for Internet-of-Things-equipped smart buildings," *IEEE Internet Things J.*, vol. 3, no. 1, pp. 96–112, Feb. 2016.

[2] W. Kang and Y. Han, "SmartPDR: Smartphone-based pedestrian dead reckoning for indoor localization," *IEEE Sensors J.*, vol. 15, no. 5, pp. 2906–2916, May 2015.

[3] Q. Tian, Z. Salcic, K. I.-K. Wang, and Y. Pan, "A multi-mode dead reckoning system for pedestrian tracking using smartphones," *IEEE Sensors J.*, vol. 16, no. 7, pp. 2079–2093, Apr. 2016.

[4] S. He and S.-H. G. Chan, "Wi-Fi fingerprint-based indoor positioning: Recent advances and comparisons," *IEEE Commun. Surveys Tuts.*, vol. 18, no. 1, pp. 466–490, 1st Quart., 2016.

[5] R. Liu *et al.*, "Collaborative SLAM based on WiFi fingerprint similarity and motion information," *IEEE Internet Things J.*, vol. 7, no. 3, pp. 1826–1840, Mar. 2020.

[6] Y. Zhuang and N. El-Sheimy, "Tightly-coupled integration of WiFi and MEMS sensors on handheld devices for indoor pedestrian navigation," *IEEE Sensors J.*, vol. 16, no. 1, pp. 224–234, Jan. 2016.

[7] L.-H. Chen, E. H.-K. Wu, M.-H. Jin, and G.-H. Chen, "Intelligent fusion of Wi-Fi and inertial sensor-based positioning systems for indoor pedestrian navigation," *IEEE Sensors J.*, vol. 14, no. 11, pp. 4034–4042, Nov. 2014.

[8] Z. Chen, Q. Zhu, and Y. C. Soh, "Smartphone inertial sensor-based indoor localization and tracking with iBeacon corrections," *IEEE Trans. Ind. Informat.*, vol. 12, no. 4, pp. 1540–1549, Aug. 2016.

[9] N. Yu, X. Zhan, S. Zhao, Y. Wu, and R. Feng, "A precise dead reckoning algorithm based on Bluetooth and multiple sensors," *IEEE Internet Things J.*, vol. 5, no. 1, pp. 336–351, Feb. 2018.

[10] Y. Li, Y. Zhuang, H. Lan, Q. Zhou, X. Niu, and N. El-Sheimy, "A hybrid WiFi/magnetic matching/PDR approach for indoor navigation with smartphone sensors," *IEEE Commun. Lett.*, vol. 20, no. 1, pp. 169–172, Jan. 2016.

[11] Y. Li, Y. Zhuang, H. Lan, P. Zhang, X. Niu, and N. El-Sheimy, "Self-contained indoor pedestrian navigation using smartphone sensors and magnetic features," *IEEE Sensor J.*, vol. 16, no. 19, pp. 7173–7182, Oct. 2016.

[12] H. Chen, F. Li, and Y. Wang, "SoundMark: Accurate indoor localization via peer-assisted dead reckoning," *IEEE Internet Things J.*, vol. 5, no. 6, pp. 4803–4815, Dec. 2018.

[13] F. Gu, S. Valaee, K. Khoshelham, J. Shang, and R. Zhang, "Landmark graph-based indoor localization," *IEEE Internet Things J.*, vol. 7, no. 9, pp. 8343–8355, Sep. 2020.

[14] A. Bose and C. H. Foh, "A practical path loss model for indoor WiFi positioning enhancement," in *Proc. 6th Int. Conf. Inf. Commun. Signal Process.*, Singapore, Dec. 2007, pp. 1–5.

[15] S. Schmitt, S. Adler, and M. Kyas, "The effects of human body shadowing in RF-based indoor localization," in *Proc. Int. Conf. Indoor Position. Indoor Navig.*, Busan, South Korea, Oct. 2014, pp. 307–313.

[16] L. Wan, G. Han, L. Shu, S. Chan, and N. Feng, "PD source diagnosis and localization in industrial high-voltage insulation system via multimodal joint sparse representation," *IEEE Trans. Ind. Electron.*, vol. 63, no. 4, pp. 2506–2516, Apr. 2016.

[17] L. E. Díez, A. Bahillo, J. Otegui, and T. Otim, "Step length estimation methods based on inertial sensors: A review," *IEEE Sensors J.*, vol. 18, no. 17, pp. 6908–6926, Sep. 2018.

[18] J. Qian, L. Pei, D. Zou, K. Qian, and P. Liu, "Optical flow based step length estimation for indoor pedestrian navigation on a smartphone," in *Proc. IEEE/ION Position Location Navig. Symp. (PLANS)*, Monterey, CA, USA, 2014, pp. 205–211.

[19] N. Roy, H. Wang, and R. R. Choudhury, "I am a smartphone and I can tell my user's walking direction," in *Proc. ACM MOBISYS*, 2014, pp. 329–342.

[20] T. Komine and M. Nakagawa, "Fundamental analysis for visible-light communication system using LED lights," *IEEE Trans. Consum. Electron.*, vol. 50, no. 1, pp. 100–107, Feb. 2004.

[21] H. L. Yang, W.-D. Zhong, C. Chen, A. Alphones, and P. Du, "QoS-driven optimized design-based integrated visible light communication and positioning for indoor IoT networks," *IEEE Internet Things J.*, vol. 7, no. 1, pp. 269–283, Jan. 2020.

[22] *LED Lighting Market to Grow to 70 Billion*, LightED Mag., St. Louis, MO, USA, 2018.

[23] S. Ma, Q. Liu, and P. C.-Y. Sheu, "Foglight: Visible light-enabled indoor localization system for low-power IoT devices," *IEEE Internet Things J.*, vol. 5, no. 1, pp. 175–185, Feb. 2018.

[24] B. Hussain, C. Qiu, and C. P. Yue, "Smart lighting control and services using visible light communication and Bluetooth," in *Proc. IEEE 8th Global Conf. Consum. Electron. (GCCE)*, 2019, pp. 1–2.

[25] M. F. Keskin, A. D. Sezer, and S. Gezici, "Localization via visible light systems," *Proc. IEEE*, vol. 106, no. 6, pp. 1063–1088, Jun. 2018.

[26] C. Danakis, M. Afgani, G. Povey, I. Underwood, and H. Haas, "Using a CMOS camera sensor for visible light communication," in *Proc. 31st IEEE GLOBECOM Workshop*, Anaheim, CA, USA, 2012, pp. 1244–1248.

[27] B. Hussain, C. Lau, and C. P. Yue, "Li-Fi based secure programmable QR code (LiQR)," in *JSAP-OSA Joint Symposia*, 2017, Art. no. 6p_A409_6. [Online]. Available: https://opg.optica.org/abstract.cfm?URI=JSAP-2017-6p_A409_6

[28] X. G. Liu, X. Wei, and L. Guo, "DIMLOC: Enabling high-precision visible light localization under dimmable LEDs in smart buildings," *IEEE Internet Things J.*, vol. 6, no. 2, pp. 3912–3924, Apr. 2019.

[29] Y.-S. Kuo, P. Pannuto, K.-J. Hsiao, and P. Dutta, "Luxapose: Indoor positioning with mobile phones and visible light," in *Proc. ACM MobiCom*, 2014, pp. 447–458.

[30] R. Zhang, W.-D. Zhong, K. Qian, and S. Zhang, "A single LED positioning system based on circle projection," *IEEE Photon. J.*, vol. 9, no. 4, pp. 1–9, Aug. 2017.

[31] Y. Hou, S. Xiao, M. Bi, Y. Xue, W. Pan, and W. Hu, "Single LED beacon-based 3-D indoor positioning using off-the-shelf devices," *IEEE Photon. J.*, vol. 8, no. 6, pp. 1–11, Dec. 2016.

[32] *Lighting of Work Places—Part 1: Indoor Work Places*, Standard EN 12464-1, 2021.

[33] Z. Li, A. Yang, H. Lv, L. Feng, and W. Song, "Fusion of visible light indoor positioning and inertial navigation based on particle filter," *IEEE Photon. J.*, vol. 9, no. 5, Oct. 2017, Art. no. 7906613.

[34] H. Huang, B. Lin, L. Feng, and H. Lv, "Hybrid indoor localization scheme with image sensor-based visible light positioning and pedestrian dead reckoning," *Appl. Opt.*, vol. 58, no. 12, pp. 3214–3221, 2019.

[35] Y. Wang and H. Zhao, "Improved smartphone-based indoor pedestrian dead reckoning assisted by visible light positioning," *IEEE Sensors J.*, vol. 19, no. 8, pp. 2902–2908, Apr. 2019.

[36] F. Gu, K. Khoshelham, C. Yu, and J. Shang, "Accurate step length estimation for pedestrian dead reckoning localization using stacked autoencoders," *IEEE Trans. Instrum. Meas.*, vol. 68, no. 8, pp. 2705–2713, Aug. 2019.

[37] J. W. Kim, H. J. Jang, D.-H. Hwang, and C. Park, "A step, stride and heading determination for the pedestrian navigation system," *J. Global Position. Syst.*, vol. 3, nos. 1–2, pp. 273–279, Dec. 2004.

[38] B. Huang, G. Qi, X. Yang, L. Zhao, and H. Zou, "Exploiting cyclic features of walking for pedestrian dead reckoning with unconstrained smartphones," in *Proc. ACM Int. Joint Conf. Pervasive Ubiquitous Comput. (UbiComp)*, 2016, pp. 374–385.

[39] H. Weinberg, *Using the ADXL202 in Pedometer and Personal Navigation Applications*, vol. 2, Analog Devices, Norwood, MA, USA, 2002, pp. 1–6.

[40] H. Gao and P. D. Groves, "Context determination for adaptive navigation using multiple sensors on a smartphone," in *Proc. ION GNSS+*, Portland, OR, USA, Sep. 2016, pp. 1–15.

[41] A. Martinelli, H. Gao, P. D. Groves, and S. Morosi, "Probabilistic context-aware step length estimation for pedestrian dead reckoning," *IEEE Sensors J.*, vol. 18, no. 4, pp. 1600–1611, Feb. 2018.

[42] Q. Wang, L. Ye, H. Luo, A. Men, F. Zhao, and C. Ou, "Pedestrian walking distance estimation based on smartphone mode recognition," *Remote Sens.*, vol. 11, no. 9, p. 1140, May 2019.

[43] Q. Wang, L. Ye, H. Luo, A. Men, F. Zhao, and Y. Huang, "Pedestrian stride-length estimation based on LSTM and denoising autoencoders," *Sensors*, vol. 19, no. 4, p. 840, Feb. 2019.

[44] J. Hannink *et al.*, "Mobile stride length estimation with deep convolutional neural networks," *IEEE J. Biomed. Health Inform.*, vol. 22, no. 2, pp. 354–362, Mar. 2018.
[45] Q. Wang *et al.*, "Personalized stride-length estimation based on active online learning," *IEEE Internet Things J.*, vol. 7, no. 6, pp. 4885–4897, Jun. 2020, doi: 10.1109/JIOT.2020.2971318.
[46] J.-S. Lee and S.-M. Huang, "An experimental heuristic approach to multi-pose pedestrian dead reckoning without using magnetometers for indoor localization," *IEEE Sensors J.*, vol. 19, no. 20, pp. 9532–9542, Oct. 2019.
[47] L. Zheng, X. Zhan, X. Zhang, S. Wang, and W. Yuan, "Heading estimation for multimode pedestrian dead reckoning," *IEEE Sensors J.*, vol. 20, no. 15, pp. 8731–8739, Aug. 2020.
[48] Q. Wang *et al.*, "Pedestrian dead reckoning based on walking pattern recognition and online magnetic fingerprint trajectory calibration," *IEEE Internet Things J.*, vol. 8, no. 3, pp. 2011–2026, Feb. 2021.
[49] F. Evennou, F. Marx, and E. Novakov, "Map-aided indoor mobile positioning system using particle filter," in *Proc. IEEE Wireless Commun. Netw. Conf.*, New Orleans, LA, USA, Mar. 2005, pp. 2490–2494.
[50] L. L. Shen and W. W. S. Hui, "Improved pedestrian dead-reckoning-based indoor positioning by RSSI-based heading correction," *IEEE Sensors J.*, vol. 16, no. 21, pp. 7762–7773, Nov. 2016.
[51] Z. Li, X. Zhao, F. Hu, Z. Zhao, J. L. C. Villacrés, and T. Braun, "SoiCP: A seamless outdoor–indoor crowdsensing positioning system," *IEEE Internet Things J.*, vol. 6, no. 5, pp. 8626–8644, Oct. 2019.
[52] R. Harle, "A survey of indoor inertial positioning systems for pedestrians," *IEEE Commun. Surveys Tuts.*, vol. 15, no. 3, pp. 1281–1293, 3rd Quart., 2013.
[53] A. R. Pratama, Widyawan, and R. Hidayat, "Smartphone-based pedestrian dead reckoning as an indoor positioning system," in *Proc. Int. Conf. Syst. Eng. Technol. (ICSET)*, Bandung, Indonesia, Sep. 2012, pp. 1–6.
[54] M. Hölzl, R. Neumeier, and G. Ostermayer, "Analysis of compass sensor accuracy on several mobile devices in an industrial environment," in *Computer-Aided Systems Theory (EUROCAST)*, R. Moreno-Díaz, F. Pichler, and A. Quesada-Arencibia, Eds. Heidelberg, Germany: Springer, 2013, pp. 381–389.

Babar Hussain (Member, IEEE) received the bachelor's degree in electronic engineering from the University of Engineering and Technology Taxila, Taxila, Pakistan, in 2012, and the M.Phil. and Ph.D. degrees in electronic and computer engineering from The Hong Kong University of Science and Technology, Hong Kong, in 2021.

He is currently a Postdoctoral Research Fellow with The Hong Kong University of Science and Technology. Based on his research work during Ph.D., he co-founded LiPHY Communications Limited, Hong Kong, in 2017 to commercialize visible light communication technology for providing location-based services in smart buildings. His research interests include optical camera communication and indoor positioning system design for consumer and robotic applications.

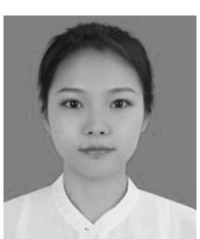

Yiru Wang (Graduate Student Member, IEEE) received the B.S. degree in communication engineering and the M.S. degree in information and communication engineering from Sun Yat-sen University, Guangzhou, China, in 2016 and 2019, respectively. She is currently pursuing the Ph.D. degree with The Hong Kong University of Science and Technology, Hong Kong.

Her research interests include visible light positioning, optical camera communication, indoor positioning systems, and robotics.

Runzhou Chen (Student Member, IEEE) received the bachelor's degree in electronic and computer engineering from The Hong Kong University of Science and Technology, Hong Kong, in 2021. He is currently pursuing the M.S. degree with the Department of Electrical Engineering, University of California at Los Angeles, Los Angeles, CA, USA.

His research interests include VLSI and analog integrated circuits and system design.

Hoi Chuen Cheng received the bachelor's degree in electronic and computer engineering from The Hong Kong University of Science and Technology, Hong Kong, in 2019.

He is currently a System and Algorithm Developer with LiPHY Communications Limited, Hong Kong. His research interests include pedestrian dead reckoning algorithm design and indoor positioning systems for consumer and robotic applications.

C. Patrick Yue (Fellow, IEEE) received the B.S. degree (Highest Hons.) in electronic and computer engineering from the University of Texas at Austin, Austin, TX, USA, in 1992, and the M.S. and Ph.D. degrees in electrical engineering from Stanford University, Stanford, CA, USA, in 1994 and 1998, respectively.

Based on his Ph.D. thesis work, he co-founded Atheros Communications, San Jose, CA, USA, in 1998 and contributed to the development and deployment of the world's first IEEE 802.11a CMOS Wi-Fi transceiver system-on-chip (SoC). In 2002, he joined Aeluros, Mountain View, CA, USA, to work on CMOS high-speed PHY/SerDes IC design and signal integrity issues in chip packaging. From 2001 to 2003, while working at the startups, he served as a Consulting Assistant Professor with the EE Department, Stanford University focusing on research in the area of high-frequency CMOS IC design and RF device modeling. In 2003, he joined Carnegie Mellon University, Pittsburgh, PA, USA, as an Assistant Professor with the Department of Electrical and Computer Engineering. In 2006, he moved to the University of California at Santa Barbara, Santa Barbara, CA, USA, and was promoted to a Full Professor in 2010. Since 2011, he has been a Professor with the Department of Electronic and Computer Engineering, The Hong Kong University of Science and Technology (HKUST). From 2014 to 2015, he served as the first Associate Provost for Knowledge Transfer with HKUST. In 2016, he took a sabbatical leave from HKUST to Tsinghua University, Beijing, China, as a Visiting Chair Professor with the Institute of Microelectronics. In 2017, he founded LiPHY Communications Limited, Hong Kong, to commercialize visible light communication technology for smart building and IoT market. He is currently the Director of the HKUST Integrated Circuit Design Center, the Optical Wireless Lab, and the HKUST-Qualcomm Joint Innovation and Research Laboratory. He has contributed to more than 200 peer-reviewed articles, 20 granted patents, and two book chapters. His research interests include optical wireless physical-layer circuits and systems, high-speed wireline communication SoC, millimeter-wave communication and sensing circuits, indoor positioning and image processing technologies for robotic applications, and edge computing accelerator design for IoT applications.

Prof. Yue was awarded the 11th Guanghua Engineering Science and Technology Youth Award by the Chinese Academy of Engineering in 2016. He and his students received the IEEE International Solid-State Circuits Conference Best Student Paper Award in 2003, the IEEE International Wireless Symposium (IWS) Best Student Paper Award in 2016, and the IEEE Circuits and Systems Society Outstanding Young Author Award in 2017. He has served on the technical program committees of the IEEE Solid-State Circuits Conference, the IEEE Symposium on VLSI Circuits (VLSI-Circuits), the IEEE RFIC Symposium, the IEEE European Solid-State Circuits Conference, the IEEE IWS, and the IEEE Asian Solid-State Circuits Conference. He was an Editor of IEEE ELECTRON DEVICE LETTERS and *IEEE Solid-State Circuits Magazine* and a Guest Editor of the IEEE TRANSACTIONS ON MICROWAVE THEORY AND TECHNIQUES. Since 2018, he has been an Editor of the PROCEEDINGS OF THE IEEE. He was an Elected AdCom Member from 2015 to 2017 for the IEEE Solid-State Circuit Society (SSCS) and was an SSCS Distinguished Lecturer from 2017 to 2018. He served as the Vice-President of Membership of the IEEE SSCS from 2016 to 2021. He is a member of ACM and a Fellow of OSA.